Since January 2020 Elsevier has created a COVID-19 resource centre with free information in English and Mandarin on the novel coronavirus COVID-19. The COVID-19 resource centre is hosted on Elsevier Connect, the company's public news and information website.

Sustainable Cities and Society 75 (2021) 103388

Contents lists available at ScienceDirect

Sustainable Cities and Society

journal homepage: www.elsevier.com/locate/scs

Spatiotemporal patterns of the COVID-19 control measures impact on industrial production in Wuhan using time-series earth observation data

Ya'nan Zhou [a,*], Li Feng [a,*], Xin Zhang [b,c], Yan Wang [a], Shunying Wang [a], Tianjun Wu [d]

[a] College of Hydrology and Water Resources, Hohai University, Address: No. 1, Xikang Road, Nanjing 210010, China
[b] Aerospace information Research Institute, Chinese Academy of Sciences, Beijing 100101, China
[c] University of Chinese Academy of Sciences, Beijing 100049, China
[d] School of Science, Chang'an University, Xi'an 710064, China

ARTICLE INFO

Keywords:
COVID-19
Industrial production
Spatiotemporal pattern
Time-series analysis
Land surface temperature

ABSTRACT

Understanding the spatiotemporal patterns of the COVID-19 impact on industrial production could improve the estimation of the economic loss and sustainable work resumption policies in cities. In this study, assuming and checking a correlation between the land surface temperature (LST) and industrial production, we applied the BFAST algorithm and linear regression models on multi-temporal MODIS data to derive monthly time-series deviation of LST with a spatial resolution of 1 × 1 km, to quantificationally explore the fine-scale spatiotemporal patterns of the COVID-19 control measures impact on industrial production, within Wuhan city. The results demonstrate that (1) the trend of time-series LST could partly reflect the impact of the COVID-19 pandemic on industrial production, and the year-around industrial production was less than expectations, with a fall of 14.30%; (2) the most serious COVID-19 impact on industrial production appeared in Mar. and Apr., then, after the lifting of lockdown, some regions (approximate 4.90%) firstly returned to expected levels in Jun, and almost all regions (98.49%) have completed the resumption of work and production before Nov.; (3) the southwest and south-central had more serious impact of the COVID-19 pandemic, approximate twice as much as that in the north and suburban, in Wuhan. The results and findings elaborated the spatiotemporal distribution and their changes during 2020 within Wuhan, which could provide a beneficial support for assessment of the COVID-19 pandemic and implementation of resumption plans for sustainable development.

1. Introduction

At the end of 2019, the sudden outbreak of the novel coronavirus disease (COVID-19) has led to a global public health disaster with hundreds of thousands of fatalities (WHO, 2021a, 2021b). To delay or prevent the spread of the disease, many affected countries implemented substantial outbreak control measures including social distancing, suspensions of public transport and industry, and widespread restrictions of movement ('lockdowns'). As the first country facing the outbreak of COVID-19 pandemic, China enacted a lockdown from 23 January to 8 April 2020 in Wuhan city where the first cases were reported, while other provinces and cities implemented strict policies to limit non-essential activities, transportation, and production since the Chinese New Year (Wang et al., 2020).

The serious COVID-19 pandemic and concomitant strict control measures lead to a significant and comprehensive impact on the public life, social and economic activities, and environments, across the world. For example, Tian et al. (2021) confirmed the continuous decreases in the domestic consumption of motor gasoline and CO_2 emissions from urban vehicles in Canada during the lockdown of the COVID-19 pandemic. World trade was expected to fall by between 13% and 32% in 2020 as the COVID-19 pandemic disrupts normal economic activity and life around the world (WTO, 2020). These in consequence affect industrial production (Shao et al., 2021), resulting in a temporary decrease of industrial productivity, and a fall of economic output. The June 2020 World Bank Global Economic Prospects reported that the COVID-19 pandemic would cause global economic output to contract by 5.2% in 2020 (World Bank, 2020).

To explore and assess these great changes and impact of the COVID-19 pandemic, many studies were carried out. These studies have mainly focused on planetary energy balance (Yi et al., 2020), air and environment quality (Lian et al., 2020; Rumpler et al., 2020; Liu et al., 2020c;

* Corresponding authors.
E-mail addresses: zhouyn@hhu.edu.cn (Y. Zhou), fly@hhu.edu.cn (L. Feng).

https://doi.org/10.1016/j.scs.2021.103388
Received 3 August 2021; Received in revised form 20 September 2021; Accepted 20 September 2021
Available online 25 September 2021

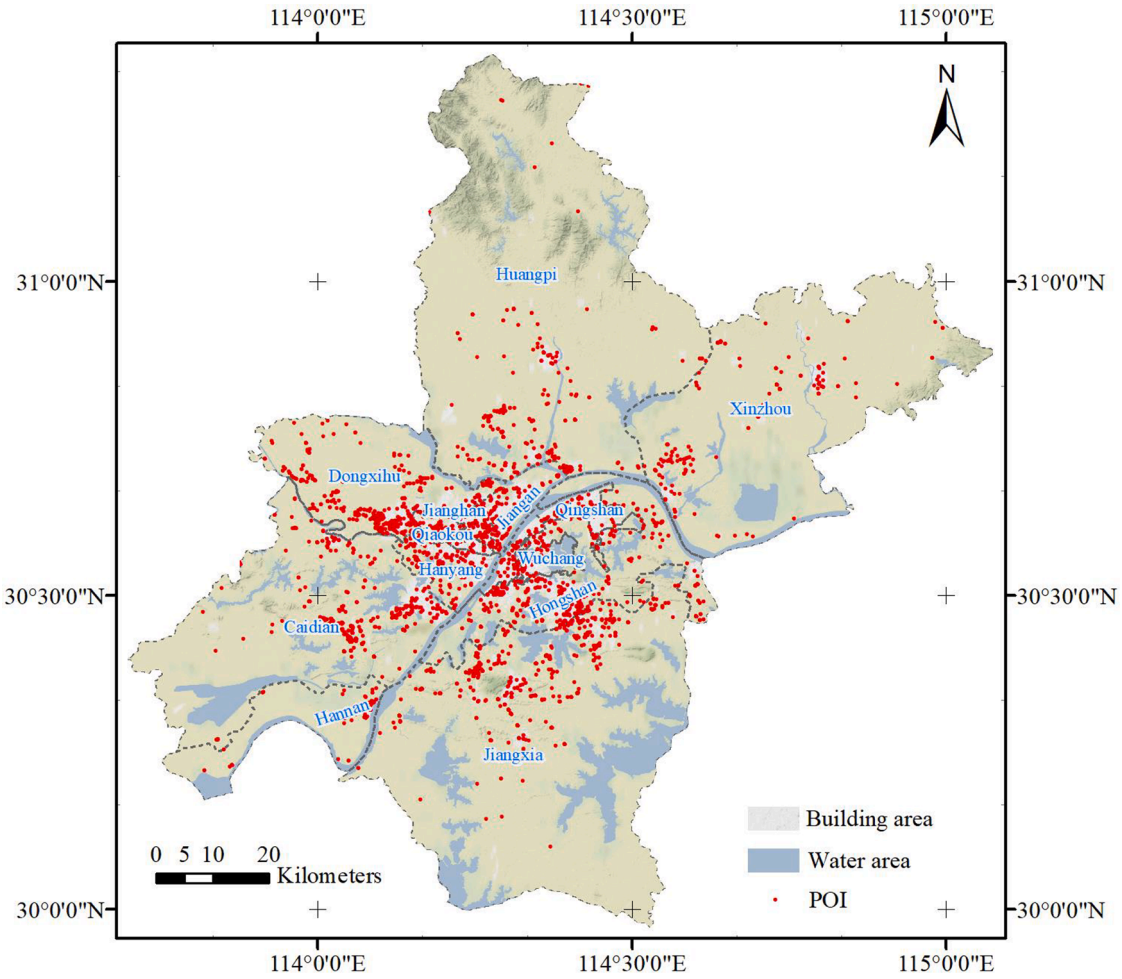

Fig. 1. Study area and POIs of high energy-consuming companies in Wuhan, China.

Chakraborty & Maity, 2020; Sathe et al., 2021; Wang & Li, 2021; Latif et al., 2021; Benchrif et al., 2021), global trade (Vidya & Prabheesh, 2020; Guan et al., 2020), travel and tourism industry (Pulella & Sica, 2021; Tian et al., 2021; Shakibaei et al., 2021; Liang et al., 2021), social and economic activity (Ehlert, 2021; Maliszewska et al., 2020), and public behaviors (Si et al., 2021). Multi-source data were used, including social economic statistical data (Sha et al., 2020; Parolin & Wimer, 2020), travelling data (Kang et al., 2020b; Jiang et al., 2021a), mobile phone data (Willberg et al., 2021; Xiong et al., 2020; Jia et al., 2020; Jadidi et al., 2021), observation and sensor data (Pulella & Sica, 2021; Liu et al., 2020b; Chen et al., 2021; Vîrghileanu et al., 2020; Basu et al., 2021), social media data (Peng et al., 2020; Li et al., 2020a; Zhu et al., 2020; Beria & Lunkar, 2021), and bibliometric data (Benita, 2021; Das & Dutta, 2021; Kutela et al., 2021). The study scales ranged from globe (Chakraborty & Maity, 2020; Laborde et al., 2020; Gupta et al., 2021), to continent and county (Fanelli & Piazza, 2020; Shi et al., 2020; Liu et al., 2020a; Kang et al., 2020b), to city and district (Tian et al., 2020; Ma et al., 2020; Liu et al., 2021). Various techniques and methods were employed, including statistic models (Chu et al., 2021; Desjardins et al., 2020), geographic mapping and spatial analysis (Shariati et al., 2020; Kang et al., 2020a; Maiti et al., 2021; Guo et al., 2021), big data and artificial intelligence (Bragazzi et al., 2020; Zhou et al., 2020; Li et al., 2020b; Ahmed et al., 2021; Ghahramani & Pilla, 2021; Chew et al., 2021).

The impact of the COVID-19 pandemic and its control measures are comprehensive for cities and society. In special, as the important social and economic activities, industrial production has decreased observably (Shao et al., 2021; Wang & Zhang, 2021) during the pandemic, which further impact the society operation and sustainable development. Through studying the spatiotemporal patterns and the long-term potential effect of the COVID-19 impact on industrial production, we can gain some valuable experience to better understand the pandemic and control measures, forecast the economic loss, which can provide sustainable evidence to guide further management and resumption. Considering the industrial process of input-production-output (and emission), population migration and urban traffic (Li et al., 2021; Xu et al., 2020), logistics (Notteboom et al., 2021), energy consumption (Jiang et al., 2021b; Wang & Zhang, 2021), night-time light imagery (Shao et al., 2021), and air contaminant (Ding et al., 2020; He et al., 2021) could be taken as indicators to partly explore the COVID-19 impact on industrial production.

Although these previous studies have greatly promoted the understanding of the COVID-19 impact on industrial production, there are a number of limitations to these approaches. (1) Available studies focused mainly on large-scale spatial analysis, such as the global emission of NOx and the urban public behaviors. There were a few studies concerning fine-scale spatial distribution and temporal trend analysis of the COVID-19 impact within cities. (2) The commonly used social and economic statistical data (such as social-media data and power consumption) within cities, are district-oriented, making it hard to locate the derived results into geographical grids. (3) Only simple multi-temporal contrastive analysis among before, during and after the lockdown was conducted, and there was a lock of comprehensive consideration on the periodic and tend components in time-series data.

From the perspective of Earth observation, satellite land surface temperature (LST) is the radiative skin temperature of the land, which

Table 1
Details of multi-temporal MODIS data.

Year	Date From	Date To	Time interval	Number of images
2017	MOD11A2.A2017001	MOD11A2.A2017361	8 days	46
2018	MOD11A2.A2018001	MOD11A2.A2018361	8 days	46
2019	MOD11A2.A2019001	MOD11A2.A2019361	8 days	46
2020	MOD11A2.A2020001	MOD11A2.A2020361	8 days	46

measures the emission of longwave thermal radiance from the land surface. LST is sensitive to changing surface conditions, including terrain, land cover, and human activities. Particularly, anthropogenic heat release can be the main cause of higher LST in urban areas compared to surrounding regions (known as urban heat island effect) (Phelan et al., 2015; Mirzaei & Haghighat, 2010). Previous studies found that the industrial areas usually experienced the highest LST in urban areas, due to heat and emission from the industrial production (especially the secondary industry and high-consuming industry) (Portela et al., 2020; Firozjaei et al., 2020; Huang & Wang, 2019). Moreover, the COVID-19 control measures disrupt and decrease the normal industrial activity (Shao et al., 2021), presenting the significant decrease in the industrial heat emission, as well as the mean LST in urban areas (Nanda et al., 2021; Parida et al., 2021). And further study also highlighted that the mean LST in industrial areas witnessed greater reduction during the COVID-19 pandemic in comparison to the average (Ali et al., 2021; Pal et al., 2021).

In this study, the LST derived from Earth observation data would be employed to explore the COVID-19 control measures impact on industrial production within Wuhan city. Specially, we applied time-series algorithms and linear regression models on four-year time-series MODIS LST data with a resolution of 1 × 1 km, to present the spatiotemporal distribution and their changes of industrial production during 2020. The contributions of this study include: (1) this is the first attempt to use LST to quantificationally measure the COVID-19 impact on industrial production, to our best knowledge, (2) Earth observation data with a resolution of 1 × 1 km was employed to capture the fine-scale spatiotemporal pattern within cities, (3) the trend component was decomposed from the time-series LST data, to calculate the LST deviation, for quantifying the change of industrial production.

The remainder of the paper is structured as follows. Section 2 presented the study area and experimental materials. In Section 3, we detailed our methods to present the spatiotemporal distribution of the LST deviation and the decrease of industrial production. Then, experiments were carried out and their spatiotemporal pattern were discussed in Section 4. Section 5 concluded this paper with several major conclusions.

2. Study area and materials

2.1. Study area

Wuhan is the capital of Hubei province, which is one of the most economically developed regions in China. It is located in the east of Jianghan Plain and the middle reaches of the Yangtze River. The Yangtze River and its largest tributary, the Han River, meet within Wuhan, forming the three towns (Wuchang, Hankou, Hanyang) across rivers. Wuhan has 13 administrative districts. And 7 districts (including Jiangan, Jianghan, Qiaokou, Hanyang, Wuchang, Qingshan and Hongshan) form the main urban area, where most of the industry is concentrated, as presented in Fig. 1.

Wuhan is a large industrial city with a relatively high proportion of heavy industry, which consume a great deal of energy, and release a large amount of heat (Gao et al., 2020). With the first confirmed of the COVID-19 pandemic and the longest lockdown, Wuhan was seriously affected. It was confirmed a fall by 4.70% of gross domestic product (GDP) and a fall by 7.30% of GDP in the secondary industry in Wuhan, due to the COVID-19 pandemic in 2020. Thus, it is important to study the spatiotemporal patterns of the COVID-19 impact on industrial production, which would support the plan for work resumptions.

2.2. Materials

MODIS LST production from 2017 to 2020, POIs of high energy-consuming companies, and annual social-economy statistical data were employed in this study to reveal the spatiotemporal patterns of the COVID-19 control measures impact on industrial production.

2.2.1. Multi-temporal MODIS LST data

The MODIS instruments capture data in 36 spectral bands ranging in wavelength from 0.405 to 14.385 μm and at three spatial resolutions (250 m, 500 m and 1 km). It views the entire surface of the Earth every one to two days. The many data products derived from MODIS observations contribute to a range of land applications including wildfire monitoring, temperature and emissivity changes, land surface change, vegetation and ecosystem dynamics, natural disasters, and agriculture studies.

In this study, the MOD11A2 Version 6 product with tile identifier of h27v05 (covering the study area) from 2017 to 2020 was obtained from MODIS Web (https://modis.gsfc.nasa.gov/) (as presented in Table 1). It provides an average 8-day LST (including both daytime and nighttime LST) in Kelvin (with a scale factor of 0.02) with a 1 km spatial resolution, for pixel-wise grid regions. We refer readers to MODIS Web for more details.

2.2.2. POIs of high energy-consuming companies

Heat discharged in the productive process (especially the high-consuming industry) would increase the surrounding LST, which makes the LST to be a potential Earth observation indicator of industrial production. Moreover, it is noted that there are other factors (such as terrain, water body and vegetation, and population density) for LST, in addition to the discharged heat. To highlight the impact on LST from industry production, as well as to weaken the diverse impacts from other factors, we further focused our study on the urban area with high-consuming industry.

In this study, POIs of high energy-consuming companies were obtained to further delineate the core study regions in the urban area within Wuhan (using method detailed in Section 3.1.2). Firstly, POIs of enterprises (including name, geographical location, and type) were gathered from the online APIs of Gaode Map (https://lbs.amap.com/api). Then, we further check their geographical locations and industry types using business databases (https://www.tianyancha.com/). Total 4710 POIs of high energy-consuming companies were obtained, as presented in Fig. 1. These POIs would be further used to spatially limit the study area in experiments.

2.2.3. Social-economy statistical data

This study made an assumption that there was a correlation relationship between the LST and industrial production (detailed in Section 3.3.1). To quantificationally measure the COVID-19 impact on industrial production and to verify their correlation, we introduced the annual GDP of the secondary industry of the whole Wuhan city and its districts (including Hannan, Dongxihu, Huangpi and Xinzhou), as well as the energy consumption of industrial enterprises above designated size, from Wuhan municipal statistics bureau (http://tjj.wuhan.gov.cn/).

3. Methodology

In this study, using time-series MODIS data, the fine-scale

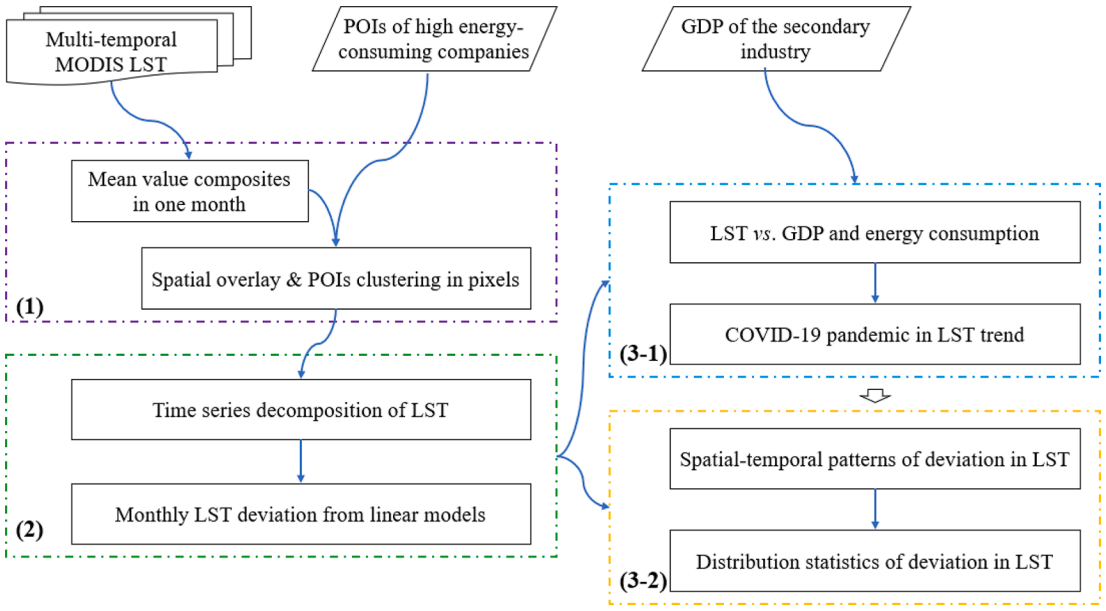

Fig. 2. Flowchart for the spatiotemporal patterns of the COVID-19 impact on industrial production, in Wuhan.

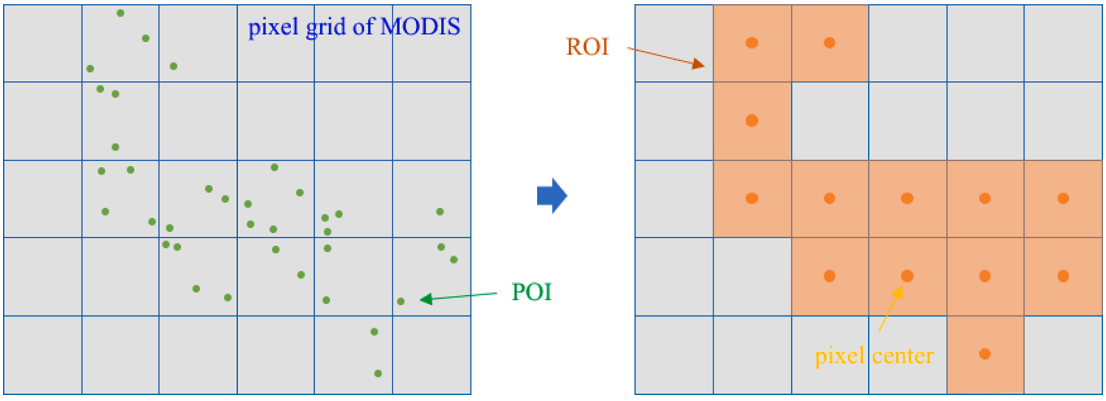

Fig. 3. POIs clustering and the pixel-wise ROIs.

spatiotemporal patterns of the COVID-19 control measures impact on industrial production were explored within Wuhan, using the flowchart presented in Fig. 2. The flowchart contained three main parts:

- Data preprocessing. We firstly used the mean value composites algorithm to composite multi-temporal 8-day MODIS data into fully-covered monthly time-series LST data. Then, on these LST data, the POIs of the secondary industry were overlaid, and spatially clustered into pixel girds to produce the region of interesting (ROI) with pixel-wise time-series LST.
- Time-series analysis. A time-series decomposition algorithm was applied on the pixel-wise time-series LST to fetch their trend component. Then following the insight of the year-over-year change, we calculated the LST deviation between the observed LST and its predicted LST for every month, in ROI.
- Spatiotemporal patterns. On the global scale of Wuhan, we firstly checked the rationality of using LST to explore the COVID-19 impact on industrial production, and further identified the monthly LST response to the COVID-19 pandemic. On the pixel scale, Spatiotemporal patterns and their distribution statistics of deviation in LST were explored.

3.1. Data preprocessing

3.1.1. Mean value composites

The MOD11A2 product provides 8-day per-pixel average LST. However, appearances of clouds and their shadows on MODIS data result in missing data. Thus, it is necessary to construct full coverage of time-series LST in the study area. Following the similar procedure of maximum value composites presented in Holben (1986), the mean value composites algorithm was applied on multi-temporal MOD11A2 product in one month to produce monthly time-series LST data, using Eq. (1).

$$\mathrm{mvc(i,j)} = \frac{1}{N(i,j)} \sum_{t=1}^{N(i,j)} v(i,j)^t \tag{1}$$

where, $N(i, j)$ is the number of effective observation (not covered by clouds and shadows) at geographical location (i, j), $v(i,j)^t$ is the pixel-wise LST value of time step t at location (i, j), $\mathrm{mvc}(i, j)$ is the final composited value at location (i, j).

The mean value composites algorithm produced regular time-series LST data. One issue that might need more attention was aligning of time steps among years, since Chinese Lunar Calendar (especially there is a difference of more than one month, in the Gregorian calendar dates of the Chinese festivals in different year) plays an important role in guiding producing activity. To eliminate this effect on the following

analysis as much as possible, we take date of the last MODIS product before the Chinese festival as the beginning of Feb. And composited MODIS data in 30 days to produce the mean-value composites LST data.

3.1.2. POIs clustering in pixel grids

Since POIs of the secondary industry have an irregular spatial distribution, it was hard (or unnecessary) to separate impact of single POI from its neighbors. Alternatively, POIs clustering in pixel grids was conducted to determine pixel-wise regions of POI impact, which were taken as regions of interest (ROI) in the following experiments and conclusions. Fig. 3 presented the procedure of POIs clustering and the pixel-wise ROIs.

3.2. Time-series analysis

3.2.1. Time-series decomposition

Previous studies mainly employed multi-temporal contrastive analysis among before, during and after the lockdown, to reveal the impacts from the COVID-19 pandemic. While, both time-series LST and industrial production demonstrate remarkable seasonal variation with one-year periods. So, we should first consider and remove the periodic component to retrieve the potential trend in time-series data, when exploring temporal changes in 2020. Detailly, time series usually contain a potential trend (overall rise or fall in the mean), seasonality (a recurring cycle), and the remaining random residual, which can be detected by time-series decomposition. Moreover, time-series decomposition also provides a structured way for time-series forecasting problem, both generally in terms of modeling complexity and specifically in terms of how to best capture each of these components in a given model.

Many algorithms were developed for time-series decomposition, including seasonal trend loess (STL) algorithm (Jacquin et al., 2010), seasonal auto-regressive integrated moving average (Jiang et al., 2010), seasonal trend analysis, and the breaks for additive season and trend (BFAST) algorithm (Verbesselt et al., 2010; Watts & Laffan, 2014). Proposed exclusively for remote-sensing datasets, BFAST algorithm can identify long term trends and abrupt changes (breaks) in time series while explicitly accounting for the seasonal component. The algorithm iteratively fits piecewise linear trend and seasonal models to a time series. The model is of the general form $Y_t = T_t + S_t + e_t$, where Y_t is the observed data at time t, T_t is the trend component, S_t is the seasonal component, and e_t is the remainder component, that is, the residual variation. The intercept and slope of the trend component model are used to derive the magnitude and direction of breaks, as well as the number of breaks and their dates. For further details, please refer to (Verbesselt et al., 2010; Watts & Laffan, 2014).

In this study, BFAST algorithm with default parameter settings was applied on the four-year (from 2017 to 2020) time-series LST data, to produce the LST trend component of and structural changes within the trend component.

3.2.2. LST deviation from linear regression

In the study period from 2017 to 2020, the COVID-19 pandemic broken out in January 2020, impacted the LST and industrial production of 2020. We assumed that the first three years (2017–2019) of LST and industrial production presented the normal change trend, while the LST in 2020 was abnormal. Further, the COVID-19 impact can be revealed by the difference between the abnormal and the predicted normal. Detailly, we firstly used the first three years of LST trend component derived from time-series decomposition, to predict the expected monthly LST in 2020, through linear regression models (*LRM*). Then, the LST deviation was defined as the difference between the observed and the predicted LST in 2020, as presented in Eqs. (2)–(4).

$$LST(i,j)^t_{pre} = LRM\left(LST(i,j)^{t,2017}_{pre}, LST(i,j)^{t,2018}_{pre}, LST(i,j)^{t,2019}_{pre}\right) \quad (2)$$

$$dev(i,j)^t = LST(i,j)^t_{obs} - LST(i,j)^t_{pre} \quad (3)$$

$$dev(i,j)^t_{map} = |dev(i,j)^t - 20| \quad (4)$$

Where $LST(i,j)^t_{obs}, LST(i,j)^t_{pre}$ are the observed LST and predicted LST at location (i, j) and in the t month of 2020, respectively. Pixel-wise deviation less than zero indicated that the observed LST was lower than the predicted, and that these pixel-wise regions has yet to recover from the COVID-19 pandemic. Further, to highlight deviation in geographic maps, we converted the predicted $dev(i,j)^t$ (having a maximum value less than 20) into $dev(i,j)^t_{map}$ for mapping in Figs. 6-10, using Eq. (4).

To further weaken the disturbance from the periodic component in one year on LST deviation, we only take the year-over-year LST in the same month to establish linear regression models. For example, observed LST of Feb. in 2017, 2018, and 2019 was used to predict LST of Feb. in 2020.

In the following exploring, the deviation of LST was taken as indicators for the COVID-19 impact on industrial production.

3.3. Spatiotemporal patterns

3.3.1. From COVID-19 pandemic to industrial production

The relationships between the LST (a proxy of the COVID-19 impact in industrial areas) and industrial production is important for exploring the COVID-19 impacts on industrial production in Wuhan. Wuhan is a large industrial city with heavy industries. The yearbook demonstrated that the secondary industry consumed approximate 59.90% energy in 2019. Industrial heat emission is one of the main heat sources in Wuhan (Huang & Wang, 2019). When operating normally, these secondary industry and heat emissions would increase the LST in industrial area (Huang & Wang, 2019; Gao et al., 2020). While, the COVID-19 pandemic decreased the industrial activities, resulting in reduction of energy consumption, as well as industrial heat emissions and lower LST in industrial areas.

By referring to previous studies (Sailor, 2011; Liao et al., 2017; Hu et al., 2020; Sun et al., 2018; He et al., 2021), we introduced and proposed four assumptions of the relationship between industrial production and LST in industrial areas: (1) industrial production is positively correlated with energy consumption; (Tang et al., 2018) (2) energy consumption is closely correlated with heat emissions; (Sun et al., 2018; He et al., 2020) (3) close correlation exists between industrial heat and secondary GDP; Sun et al., 2018; He et al., 2020) (4) the industrial heat emissions is also positively correlated with the LST in industrial areas (Huang & Wang, 2019; Gao et al., 2020). Based on these assumptions, we can employ the LST to represent industrial activities, and further detail the spatiotemporal changes of LST to explore the COVID-19 impacts on industrial production in Wuhan.

3.3.2. Hot spot analysis

Hot spot analysis uses statistical analysis (calculating the Getis-Ord Gi* statistic) to define areas (features) with either high or low values cluster spatially. In hot spot analysis, to be a statistically significant hot spot, a feature (region) will have a high value and be surrounded by other features with high values as well. The local sum for a feature and its neighbors are compared proportionally to the sum of all features. When the local sum is very different from the expected local sum, and when that difference is too large to be the result of random chance, a statistically significant score results.

In this study, we used the optimized hotspot analysis tool in ArcGIS to illustrate the spatial clustering distribution of high and low impact from the COVID-19 pandemic by calculating the GI bin index. The Gi_Bin field identifies statistically significant hot and cold spots, corrected for multiple testing and spatial dependencies using the false discovery rate correction method. Features with a Gi_Bin value of either +3 or −3 were

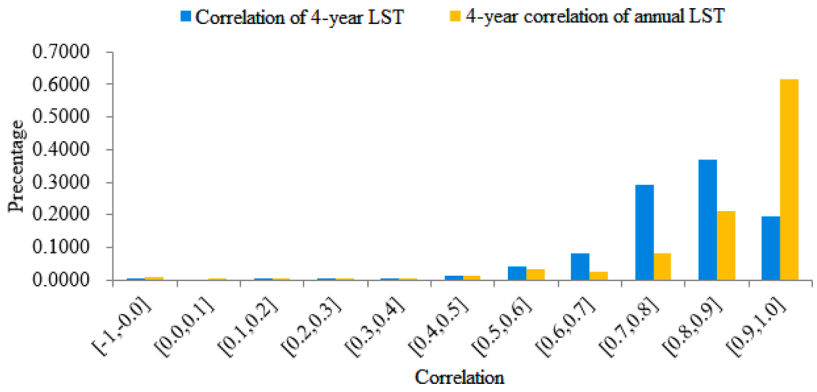

Fig. 4. Correlation between LST in daytime and nighttime.

Table 2
Annual LST and secondary GDP and energy consumption and their prediction.

Year	2017	2018	2019	2020	*2020 prediction*
Mean LST (K)	299.62	299.56	299.90	299.66	*299.98*
2nd GDP (Billion)	5227.00	5861.00	6377.00	5557.00	*6481*
Energy (10000 ton)	5233.69	5289.77	5354.99	5264.87	\

statistically significant at the 99% confidence level (CI); +/−2 bins 95% CI; +/−1 bins 90% CI. Features with 0 were not statistically significant.

3.3.3. Statistical analysis on LST

Based on the results of LST deviations and their hot spots, we conducted more statistical analysis, to further quantificationally reveal the spatiotemporal changes of the COVID-19 impact on industrial production. Through calculating the largest minus deviation and accumulated deviation for every pixel, we can identify the month with the greatest monthly impact and pixel-wise regions with greatest annual impact from the COVID-19 pandemic. The statistic on the month of the last minus deviation, indicated the fading of the impact on industrial production.

4. Experiments and discussion

Global-scale trend and verification were firstly conducted to ensure the effectiveness of our study. Then fine-scale spatiotemporal distributions and their statistics of LST deviation were presented and discussed.

4.1. Regional LST trend in COVID-19 pandemic

4.1.1. LST in daytime or nighttime

MOD11A2 Version 6 product provides daytime and nighttime LSTs. Before conducting spatiotemporal analysis on LSTs during the COVID-19 pandemic, we should make clear which LST (or their combination) can reveal the changes of industrial production.

We firstly compared the different factors of LSTs in daytime and nighttime, in theory. Compared with the nighttime LST, the daytime LST has exclusive solar radiation and more human activities (including public living and production), resulting in a higher LST in daytime. Then, let's take a close look on the solar radiation and human activities. In the four years, we can assume that the annual cycle of solar radiation is stable, and the monthly solar radiation (we used the monthly LST in our experiments) has the same annual cycle. This stable annual cycle of the solar radiation would product a horizontal line of the trend components in the time-series decomposition. Although there is great difference between human activities in daytime and nighttime (such as building industry), whose difference also shares stable annual cycles in local regions. This kind of difference would also generate a horizontal line of trend in the BFAST algorithm. This is, the difference between daytime and nighttime LSTs is nearly periodic, and there is little difference to use daytime or nighttime LST to explore the changes of industrial production.

In experiments, we further checked the possible difference in using daytime or nighttime LSTs. Firstly, we extracted trend components of nighttime LST for every pixel in the ROIs. Then, correlation coefficients (including correlation of four-year LST and four-year correlation of annual LST) between daytime and nighttime time-series LSTs were calculated and analyzed, as presented in Fig. 4. There were approximate 90.97% pixel-wise regions having highly corrected annual daytime and nighttime LSTs (with correlation coefficient greater than 0.7), and 85.19% regions for the four-year LSTs. The results further showed that both daytime and nighttime LSTs can be used to explore the changes of industrial production.

Let's take a close look at the methodology, time-series decomposition

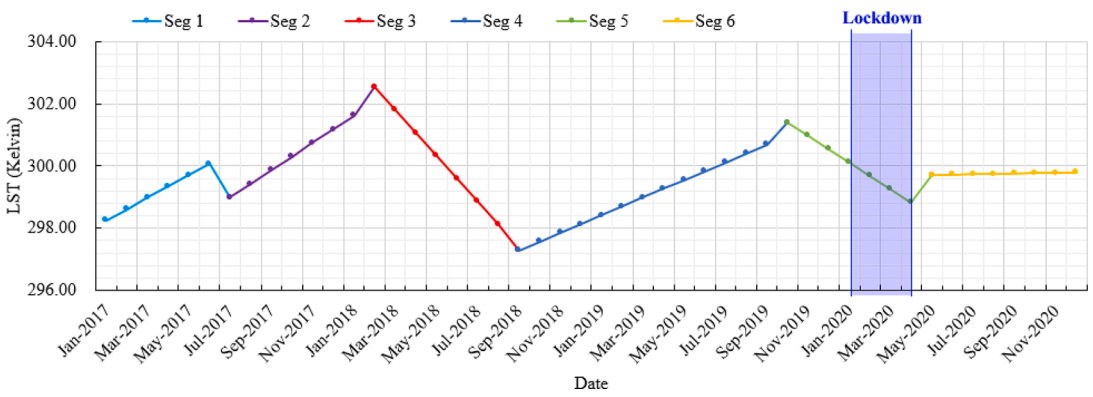

Fig. 5. The trend component of the mean time-series LST data in Wuhan.

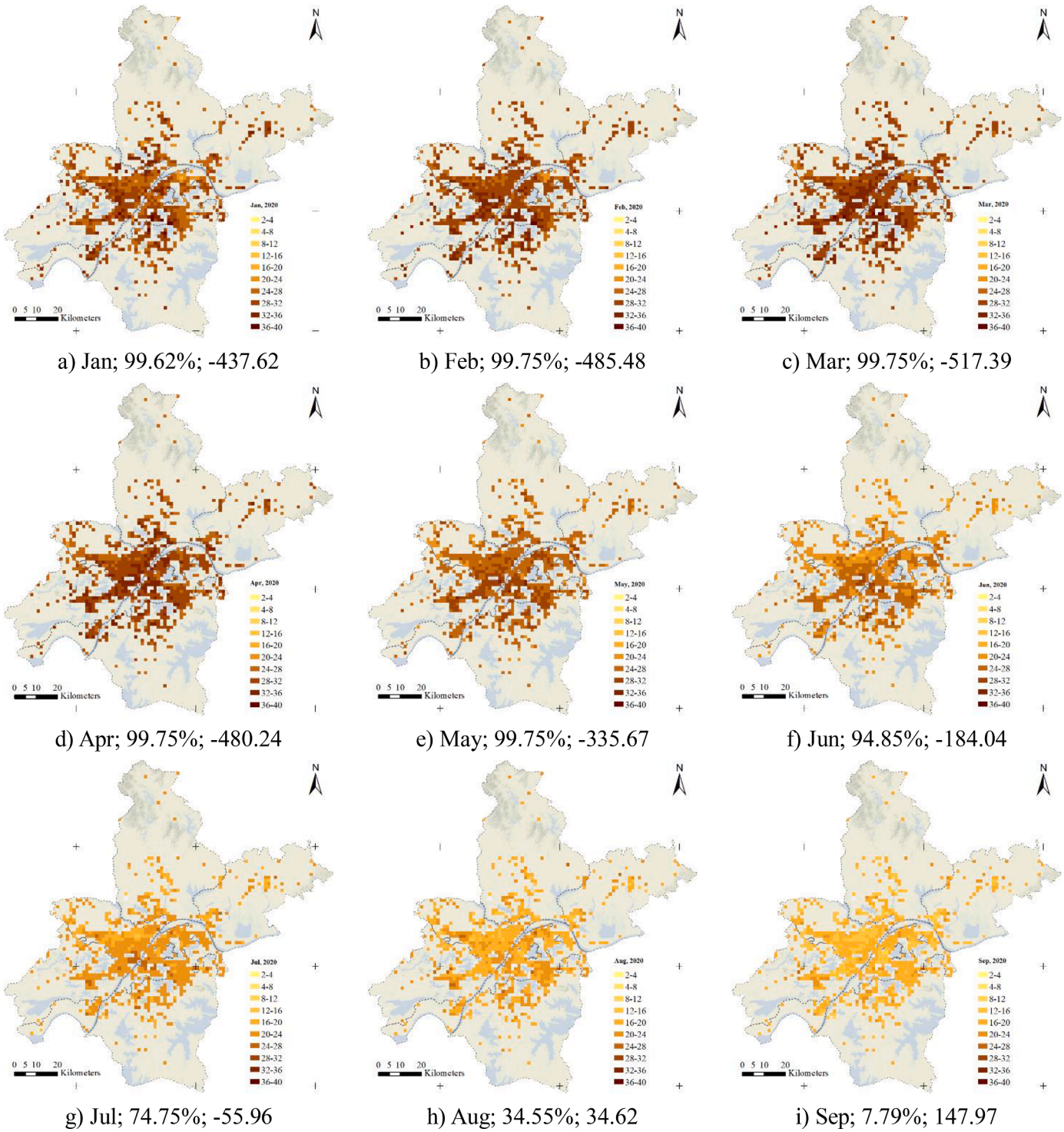

Fig. 6. Spatiotemporal distribution of LST deviation of 2020, in Wuhan. The values in the blow text indicated the percentage of minus deviation and the monthly mean deviation.

on time-series LST separate the periodic components (annual natural and human-induced changes), and keep only the trend components. The trend components could accurately present the changes of LST trend during the COVID-19 pandemic. This is exactly one contribution of our study, compared with previous studies on the COVID-19 impact. In the following spatiotemporal analysis, we only employed the time-series LST in daytime.

4.1.2. LST trend vs. secondary GDP and energy consumption

Taking the GDP of the secondary industry and energy consumption of industrial enterprises above designated size (energy consumption) as the measurable proxy of the industrial production, we verified the correlation relationship between LST and industrial production, using the annual mean LST, and the secondary GDP and energy consumption in the four years (as presented in Table 2).

For the whole Wuhan city (in the ROIs), the correlation coefficient

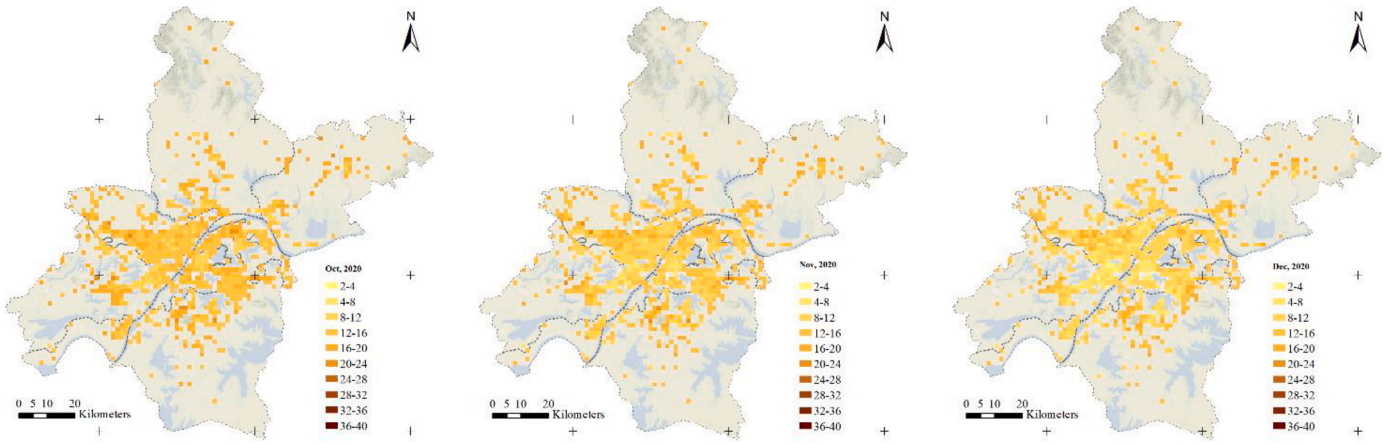

j) Oct; 1.88%; 256.96 k) Nov; 1.26%; 351.28 l) Dec; 0.00%; 430.45

Fig. 6. (*continued*).

between the mean LST and the secondary GDP, and between the mean LST and energy consumption, were 0.7386 and 0.7984, respectively. These greater correlations supported these assumptions detailed in section 3.3.1, that the LST can partly present the industrial production in Wuhan. Then, pixel grids in the ROIs were assigned to the administrative districts of Wuhan. In districts with available GDP data, correlation coefficients also were calculated, by the similar procedure. The results showed the correlation coefficients ranged from 0.6404 to 0.7077, also suggesting that LST can be employed to reveal the COVID-19 impact on industrial production.

Furthermore, we tried to quantify the actual impact of the COVID-19 pandemic on industrial production. Firstly, a linear regression model (from Year to Mean LST) derived from the first three years of annual mean LST, was used to predict the mean LST of 2020 of 299.98, as presented in the last column in Table 2. Then, we employed a linear regression model (from Mean LST to GDP) to predict the GDP in 2020 of 6481. Finally, comparing the actual and the predicted, a fall of 14.30% in GDP of the secondary industry was calculated.

4.1.3. COVID-19 pandemic in LST trend

Feeding the monthly mean time-series LST from 2017 to 2020 in the ROIs, into the BFAST algorithm, we obtained its trend component and structural changes, as presented in Fig. 5.

Although the trend component of time-series LST had a small variation range (from 297.28 to 302.52, 5.24 Kelvin), it presented obvious structural changes, with six segments. The control measures of COVID-19 pandemic (from Jan. 23 to Apr. 8 in 2020) were conducted in Seg5, and the continuing impact appeared in Seg6.

Let's take a close look at the Seg5 and Seg6. The Seg5 (from Oct. 2019 to May 2020) demonstrated an obvious descent in LST, which was mainly dominated by the COVID-19 lockdown. In special, during the lockdown, the LST continued to decrease, and reached the lowest point in Apr. After the lifting of lockdown on Apr. 8, the LST began to rise in May. Then, from May to Dec. (Seg6), the LST presented a slight increase, along the work resumptions after lockdown. These findings qualitatively verified that the changes of time-series LST can partly reflect the impact of the COVID-19 pandemic on industrial production.

4.2. Spatiotemporal distribution of LST deviation

4.2.1. Spatiotemporal distribution of deviation

Following the procedure detailed in Section 3.2, monthly pixel-wise LST deviations were calculated for the pixel-wise ROIs (and the following spatiotemporal exploring is also confirmed to the ROIs). The spatiotemporal distribution of LST deviation were presented in Fig. 6.

As a whole, there was an obvious change in LST deviation, first lowering and then recovering in 2020. In details, the LST deviation firstly increased from Jan. to Mar. and Apr., indicating the increasing COVID-19 impact on industrial production. This was expected, since the lockdown continued into Apr. in Wuhan. Then, after the lifting of the lockdown, the LST deviation reduced sharply, and reached zero in Jul. and Aug. This suggested that the industrial production has returned back to their expected levels. Then, the LST deviation began to be positive in Aug., and increase sharply, from Sep. to Dec., which was a big rebound of industrial production, after the COVID-19 pandemic. Taking a close look at the recovery procedure, the LST recovery after the lifting of the lockdown in Apr. was remarkable faster than its attenuation process from Jan. to Apr. The LST deviation in May began to be greater than that in the beginning of the lockdown, due to the large demand unfulfilled during the lockdown in industrial production.

From the perspective of the percentage of minus deviation (showed in the blow text of sub figures in Fig. 6), almost all regions have minus deviations (greater than 99.00%) before May, indicating that the COVID-19 pandemic affected the total industrial production in Wuhan. From Jun. to Sep., the percentages of minus deviation reduce sharply from 94.85% to 7.79%, presenting the fading of the COVID-19 impact. After Oct., industrial production in almost all regions (98.49%) has almost recovered to the expected.

4.2.2. Hot spot of the LST deviation

Hot spot analysis algorithm was applied on the spatial distribution of LST deviation in the pixel-wise ROIs to identify their hop spot regions and changes, as presented in Fig. 7. As a whole, the area of the hot spot regions presented a changing process of first growth and then dissipation. And the spatial location of hot spot has a development process of first from suburban to downtown, and then to suburban.

More specifically, hot spot mainly distributed in small regions in the southwest and south of the ROIs, at the beginning of the COVID-19 pandemic in Jan. In Feb., hot spot spread rapidly in the southwest and south, with a higher confidence. In Mar., hot spot further spread to the north, covering the center of the ROIs. In Apr. there was a little change in spatial area, but a large promotion in confidence, indicating more serious impact in hot spot regions than that in other area. In May, hot spot persistently appeared in the southwest, south, southeast, and south center, while the north party of center recovered to be the no-significant. In Jun. and Jul., the hot spot spread into more suburban in the east and south, but with a decreasing confidence. While, the cold spot always congregated in the suburbs from Jan. to Jul. In Aug., hot spot of LST deviation began to flinch from the center, and the cold spot began to gather in the north, indicating a relative quick and effective work

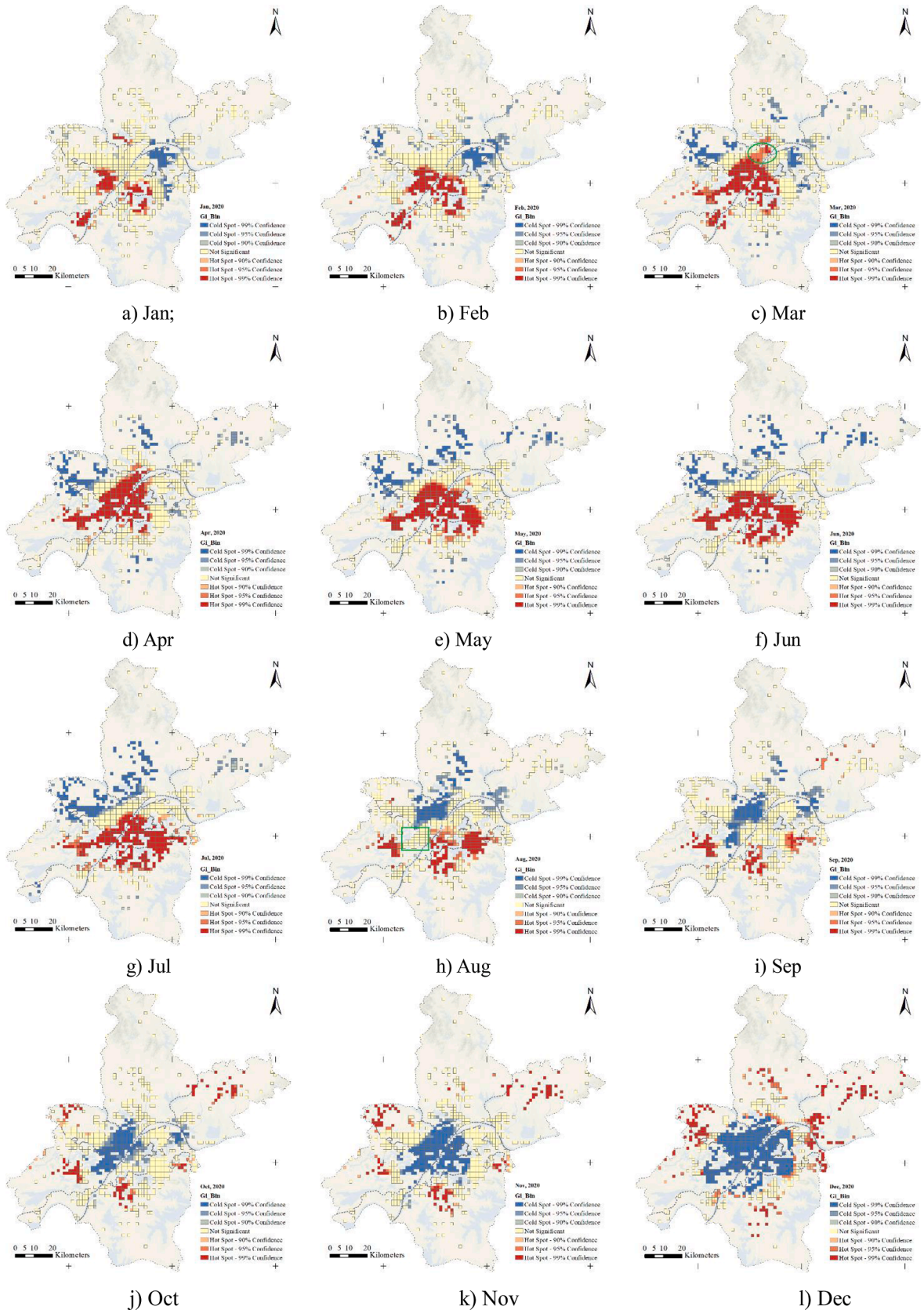

Fig. 7. Hot spot regions and its changes of LST deviation of 2020, in Wuhan (For interpretation of the references to color in this figure, the reader is referred to the web version of this article).

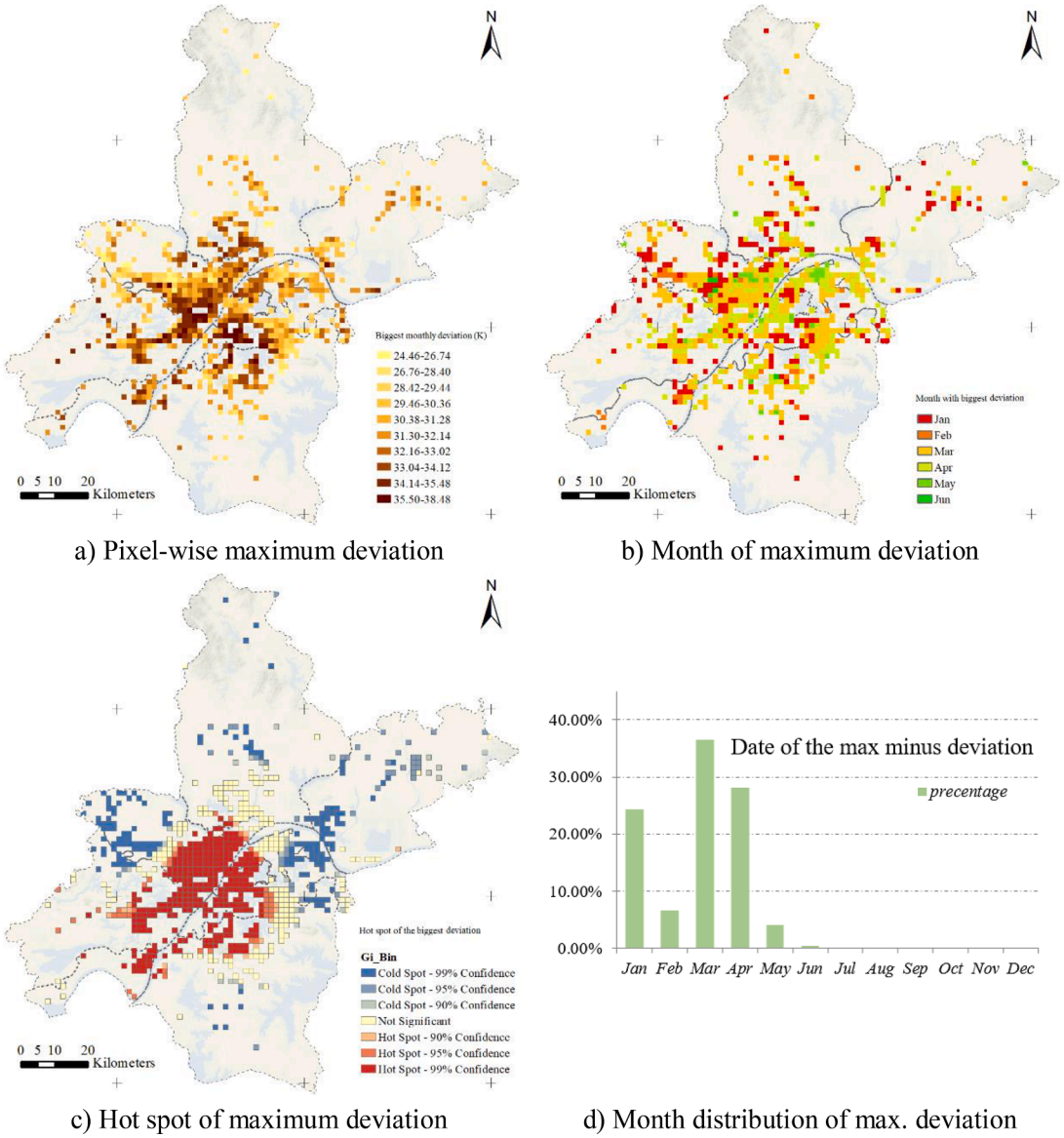

Fig. 8. Pixel-wise maximum LST deviation and their corresponding date.

resumption. In Sep., hot spot only remained in the small area in the southwest, south, and southeast, while cold spot continued to expand. From Oct. to Dec., hot spot continuously faded, while the cold spot continuously spread, covering the center of the ROIs.

There were several key temporal turning points in the spatial distribution. In Mar. and Apr., hot spot concentrated in the center, along the banks of Yangtze river, indicating that the center had a more serious impact than the suburban. In Jun. and Jul., regions with more serious impact were distributed in the south of city. And after Oct., the impact of the COVID-19 pandemic transferred to the suburban.

And several diverse spatial regions were indicated in the spatial distribution of hot spot. One was the Jiang'an District, labeled with a green circle in figure (c) in Fig. 7. In Mar. and Apr., the hot spot region covered this area, and changed to be the no-significant in May, which indicated that it was the first regions with work resumption. The second is in Hanyang District, labeled with a green box in figure (h) in Fig. 7. Before Aug., it was always in hot spot. Then it transferred to no-significant regions in Aug., and to cold spot in Sep. This presented a rapid work resumption.

4.3. Distribution statistics of LST deviation

4.3.1. The largest minus deviation

Based on the spatiotemporal distribution of the deviations in LST, we further conducted the maximum statistical analysis for every pixel in the ROIs, and the results were presented in Fig. 8.

In Fig. 8, figure (a) and (c) demonstrated the pixel-wise maximum LST deviation and its hot spot region, respectively. The more serious monthly impact of the COVID-19 pandemic was mainly distributed in the center and southwest of the ROIs.

In the view of the month of maximum deviation in figure (b), both the northwest and suburban first faced the maximum deviation in Jan. and Feb., while, the maximum deviation of downtown (regions along the river bank, in special) appeared in Apr. to Jun. figure (d) presented the month distribution of pixel-wise maximum deviation. In Mar. and Apr., approximate 64.57% regions have their maximum deviation. It was expected, since as the lockdown continued, industrial production would be increasingly affected. In special, Mar. has a greater percentage of maximum deviation than Apr., with the possible reason is the lifting of lockdown in the early of Apr. Furthermore, there were few regions with the maximum deviation after Jun.

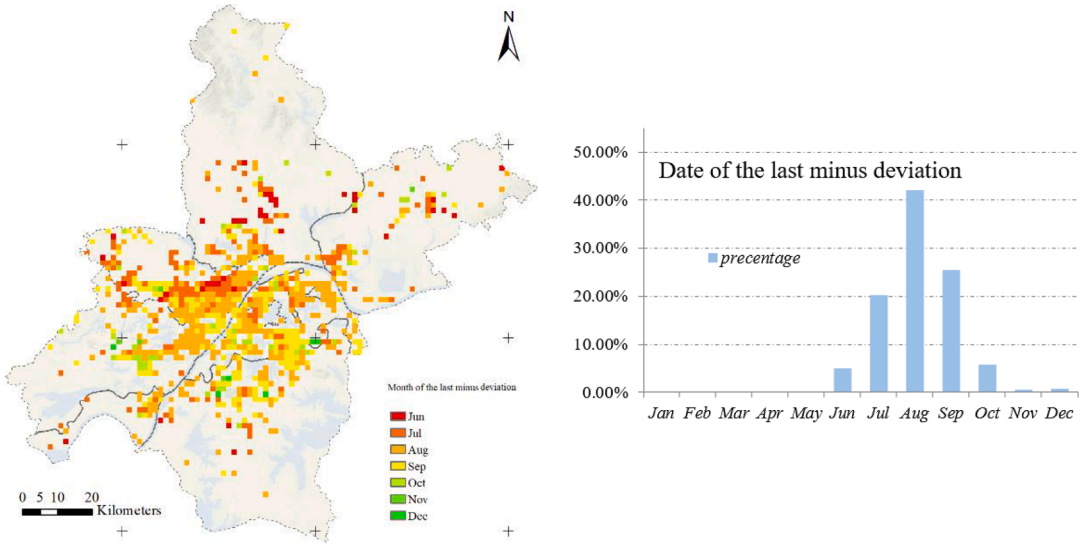

a) Spatial distribution of the last month of the minus deviation

b) Month distribution of the last month of the minus deviation

Fig. 9. Spatiotemporal pattern of the last minus deviation.

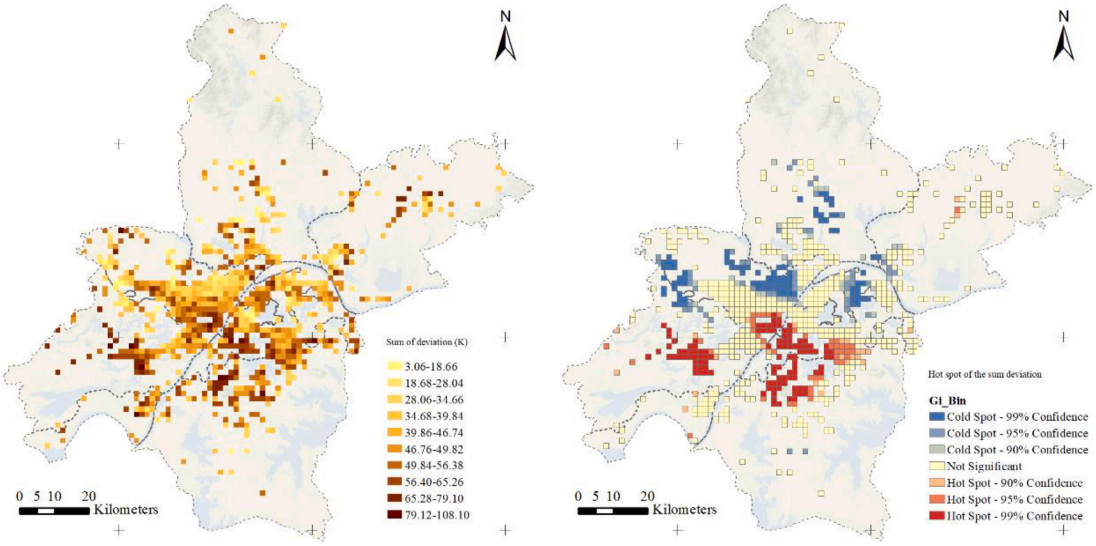

a) Accumulation of all deviation in LST

b) Hot spot of accumulation of all deviation

Fig. 10. spatiotemporal pattern of the accumulation of deviation.

4.3.2. The month of the last minus deviation

The last minus deviation indicated the end of the COVID-19 impact on LST and industrial production, and the LST and industrial production has achieved or surpassed the expectations. Based on the spatiotemporal distribution of the LST deviation, we further found the last minus deviation for every pixel in the ROIs, and the results were presented in Fig. 9.

In Fig. 9, figure (a) demonstrated the spatial distribution of the last month of the minus deviation. In Jun. (approximate 4.90% in figure (b)) and Jul. (approximate 20.23%), the north region has first gotten rid of the impact of the COVID-19 pandemic, and returned to expected levels. There were most regions (approximate 42.09%) back to expectations in Aug., which are mainly located along the river bank. Before Nov., almost all the regions (98.49%) have completed the resumption of work and production.

4.3.3. The accumulation of deviation

The accumulation of LST deviation (including both plus and minus deviation in 2020) could indicate the annual impact of the COVID-19 pandemic on industrial production. The results in the ROIs were presented in Fig. 10.

As a whole, there were approximate 95.73% regions with an accumulation of deviation less than zero, indicating that annual industrial production in almost all regions was less than expectations, in spite of the strong rebound after the lifting of the lockdown in Apr.

In details of figure (b), regions with greater accumulation of deviation were mainly located in the southwest and south-central of the ROIs, while the north and suburban have relatively small accumulated deviation. We further calculated the mean accumulated LST deviation in hot spot regions and cold spot regions with greater confidence than 95%, respectively. The results showed that the hot spot regions have a mean accumulated LST deviation of 15.35, twice of that in cold spot regions

with a mean deviation of 7.94, which partly suggested the degrees of the COVID-19 impact on industrial production of the two significant regions.

5. Conclusion

To study the impact of the COVID-19 pandemic on industrial production (reflected by the land surface temperature), we derived monthly time-series LST deviation with a spatial resolution of 1 × 1 km in the ROIs of high-consuming industry within Wuhan city in 2020, by applying the BFAST algorithm and linear regression models to multi-temporal MODIS observation. Through exploring the monthly pixel-wise LST deviation between the observed and the predicted from the multi-year trend, we quantified the detailed spatiotemporal pattern of the COVID-19 impact on industrial production. From the results of the experiments and statistics in the ROIs, we mainly concluded: (1) the remote sensing data with time-series analysis technique can reveal the fine-scale spatiotemporal changes of the COVID-19 impact within urban areas. (2) Taking Wuhan city in 2020 as a whole, the trend of time-series LST could partly reveal the impact of the COVID-19 pandemic on industrial production. The year-around industrial production in Wuhan was less than expectations, with a fall of 14.30%. (3) From the temporal perspective, in Mar. and Apr., approximate 64.57% regions have their monthly maximum deviation and the most serious impact on industrial production. After the lifting of lockdown, some regions (approximate 4.90%) firstly returned to expected levels in Jun, and there were most regions (approximate 42.09%) back to expectation in Aug., and almost all regions (98.49%) have completed the resumption of work and production, before Nov. (4) From the spatial view, regions with more serious impact of the COVID-19 pandemic were mainly located in the southwest and south-central, while the north and suburban have relatively small impact (a half of that in the southwest and south-central). The spatial location of hot spot regions developed from the southwest to the center, and shrink to the south, and fade away in the suburban.

In short, there were great decrease in the whole industrial production, and significant differences in spatiotemporal distribution of the industrial production loss and their resumption caused by the COVID-19 pandemic within Wuhan City. Our study suggests that administrators and planner should rethink the impacts of control measures during pandemics, and guide measures for work resumption after pandemics, from a finer spatiotemporal perspective. It is not rational to immediately drop enforcement measures. But more elaborate monitoring and adaptive measures are needed for the next wave of possible pandemic (for example, how to regionally and timely conduct control measures and plans of work resumption), for the accurate estimation of the economic loss and the reducing of the COVID-19 impact on industrial production. Moreover, the selected LST in this study could partly represent the spatiotemporal changes of industrial production. Authors believe that further investigations with more spatiotemporal big data (Zhou et al., 2020) are needed to promote these analytics for sustainable cities.

Declaration of Competing Interest

The authors declare that they have no known competing financial interests or personal relationships that could have appeared to influence the work reported in this paper.

Funding

This work was supported in part by the National Key Research and Development Program under Grant 2019YFC1804301, the National Natural Science Foundation of China under Grant No. 42071316, Key Laboratory of National Geographic Census and Monitoring, Ministry of Natural Resources under Grant No. 2020NGCM03, Open Fund of State Key Laboratory of Remote Sensing Science under Grant No. OFSLRSS201919, the Fundamental Research Funds for the Central Universities under Grant No. B200202008, the Opening Foundation of Key Lab of Spatial Data Mining & Information Sharing, Ministry of Education (Fuzhou University) under Grant No. 2019LSDMIS04.

Availability of data and materials

The data that support the findings of this study are available upon request by contact with the corresponding author.

Reference

Ahmed, I., Ahmad, M., & Jeon, G. (2021). Social distance monitoring framework using deep learning architecture to control infection transmission of COVID-19 pandemic. *Sustainable Cities and Society, 69*, Article 102777.

Ali, G., Abbas, S., Qamer, F. M., et al. (2021). Environmental impacts of shifts in energy, emissions, and urban heat island during the COVID-19 lockdown across Pakistan. *Journal of Cleaner Production, 291*, Article 125806.

Basu, B., Murphy, E., Molter, A., et al. (2021). Investigating changes in noise pollution due to the COVID-19 lockdown: The case of Dublin, Ireland. *Sustainable Cities and Society, 65*, Article 102597.

Benchrif, A., Wheida, A., Tahri, M., et al. (2021). Air quality during three covid-19 lockdown phases: AQI, PM2. 5 and NO2 assessment in cities with more than 1 million inhabitants. *Sustainable Cities and Society, 74*, Article 103170.

Benita, F. (2021). Human mobility behavior in COVID-19: A systematic literature review and bibliometric analysis. *Sustainable Cities and Society, 70*, Article 102916.

Beria, P., & Lunkar, V. (2021). Presence and mobility of the population during the first wave of Covid-19 outbreak and lockdown in Italy. *Sustainable Cities and Society, 65*, Article 102616.

Bragazzi, N. L., Dai, H., Damiani, G., et al. (2020). How big data and artificial intelligence can help better manage the COVID-19 pandemic. *International Journal of Environmental Research and Public Health, 17*(9), 3176.

Chakraborty, I., & Maity, P. (2020). COVID-19 outbreak: Migration, effects on society, global environment and prevention. *Science of the Total Environment, 728*, Article 138882.

Chen, Y., Qin, R., Zhang, G., et al. (2021). Spatial temporal analysis of traffic patterns during the COVID-19 epidemic by vehicle detection using planet remote-sensing satellite images. *Remote Sensing, 13*(2), 208.

Chew, A. W. Z., Wang, Y., & Zhang, L. (2021). Correlating dynamic climate conditions and socioeconomic-governmental factors to spatiotemporal spread of COVID-19 via semantic segmentation deep learning analysis. *Sustainable Cities and Society*, Article 103231.

Chu, A. M. Y., Chan, J. N. L., Tsang, J. T. Y., et al. (2021). Analyzing cross-country pandemic connectedness during COVID-19 using a spatial-temporal database: Network analysis. *JMIR Public Health and Surveillance, 7*(3), e27317.

Das, S., & Dutta, A. (2021). Characterizing public emotions and sentiments in COVID-19 environment: A case study of India. *Journal of Human Behavior in the Social Environment, 31*(1-4), 154–167.

Desjardins, M. R., Hohl, A., & Delmelle, E. M. (2020). Rapid surveillance of COVID-19 in the United States using a prospective space-time scan statistic: Detecting and evaluating emerging clusters. *Applied Geography, 118*, Article 102202.

Ding, J., van der, A. R. J., Eskes, H. J., et al. (2020). NOx emissions reduction and rebound in China due to the COVID-19 crisis. *Geophysical Research Letters, 47*(19). e2020GL089912.

Ehlert, A. (2021). The socio-economic determinants of COVID-19: A spatial analysis of German county level data. *Socio-Economic Planning Sciences*, Article 101083.

Fanelli, D., & Piazza, F. (2020). Analysis and forecast of COVID-19 spreading in China, Italy and France. *Chaos, Solitons & Fractals, 134*, Article 109761.

Firozjaei, M. K., Weng, Q., Zhao, C., et al. (2020). Surface anthropogenic heat islands in six megacities: An assessment based on a triple-source surface energy balance model. *Remote Sensing of Environment, 242*, Article 111751.

Gao, S., Zhan, Q., Yang, C., et al. (2020). The diversified impacts of urban morphology on land surface temperature among urban functional zones. *International Journal of Environmental Research and Public Health, 17*(24), 9578.

Ghahramani, M., & Pilla, F. (2021). Leveraging artificial intelligence to analyze the COVID-19 distribution pattern based on socio-economic determinants. *Sustainable Cities and Society, 69*, Article 102848.

Guan, D., Wang, D., Hallegatte, S., et al. (2020). Global supply-chain effects of COVID-19 control measures. *Nature Human Behaviour, 4*(6), 577–587.

Guo, Y., Qian, H., Sun, Z., et al. (2021). Assessing and controlling infection risk with Wells-Riley model and spatial flow impact factor (SFIF). *Sustainable Cities and Society, 67*, Article 102719.

Gupta, A., Bherwani, H., Gautam, S., et al. (2021). Air pollution aggravating COVID-19 lethality? Exploration in Asian cities using statistical models. *Environment, Development and Sustainability, 23*(4), 6408–6417.

He, C., Yang, L., Cai, B., et al. (2021). Impacts of the COVID-19 event on the NOx emissions of key polluting enterprises in China. *Applied Energy, 281*, Article 116042.

He, C., Zhou, L., Yao, Y., et al. (2020). Estimating spatial effects of anthropogenic heat emissions upon the urban thermal environment in an urban agglomeration area in East China. *Sustainable Cities and Society, 57*, Article 102046.

Holben, B. N. (1986). Characteristics of maximum-value composite images from temporal AVHRR data. *International Journal of Remote Sensing, 7*(11), 1417–1434.

Hu, D., Meng, Q., Zhang, L., et al. (2020). Spatial quantitative analysis of the potential driving factors of land surface temperature in different “Centers” of polycentric

cities: A case study in Tianjin, China. *Science of The Total Environment, 706*, Article 135244.
Huang, X., & Wang, Y. (2019). Investigating the effects of 3D urban morphology on the surface urban heat island effect in urban functional zones by using high-resolution remote sensing data: A case study of Wuhan, Central China. *ISPRS Journal of Photogrammetry and Remote Sensing, 152*, 119–131.
Jacquin, A., Sheeren, D., & Lacombe, J. P. (2010). Vegetation cover degradation assessment in Madagascar savanna based on trend analysis of MODIS NDVI time series. *International Journal of Applied Earth Observation and Geoinformation, 12*, S3–S10.
Jadidi, M. M., Jamshidiha, S., Masroori, I., et al. (2021). A two-step vaccination technique to limit COVID-19 spread using mobile data. *Sustainable Cities and Society, 70*, Article 102886.
Jia, J. S., Lu, X., Yuan, Y., et al. (2020). Population flow drives spatio-temporal distribution of COVID-19 in China. *Nature, 582*(7812), 389–394.
Jiang, B., Liang, S., Wang, J., et al. (2010). Modeling MODIS LAI time series using three statistical methods. *Remote Sensing of Environment, 114*(7), 1432–1444.
Jiang, P., Fu, X., Van Fan, Y., et al. (2021a). Spatial-temporal potential exposure risk analytics and urban sustainability impacts related to COVID-19 mitigation: A perspective from car mobility behaviour. *Journal of cleaner production, 279*, Article 123673.
Jiang, P., Van Fan, Y., & Klemeš, J. J. (2021b). Impacts of COVID-19 on energy demand and consumption: Challenges, lessons and emerging opportunities. *Applied Energy, 285*, Article 116441.
Kang, D., Choi, H., Kim, J. H., et al. (2020a). Spatial epidemic dynamics of the COVID-19 outbreak in China. *International Journal of Infectious Diseases, 94*, 96–102.
Kang, Y., Gao, S., Liang, Y., et al. (2020b). Multiscale dynamic human mobility flow dataset in the US during the COVID-19 epidemic. *Scientific Data, 7*(1), 1–13.
Kutela, B., Novat, N., & Langa, N. (2021). Exploring geographical distribution of transportation research themes related to COVID-19 using text network approach. *Sustainable Cities and Society, 67*, Article 102729.
Laborde, D., Martin, W., Swinnen, J., et al. (2020). COVID-19 risks to global food security. *Science, 369*(6503), 500–502.
Latif, M. T., Dominick, D., Hawari, N. S. S. L., et al. (2021). The concentration of major air pollutants during the movement control order due to the COVID-19 pandemic in the Klang Valley, Malaysia. *Sustainable Cities and Society, 66*, Article 102660.
Li, C., Chen, L. J., Chen, X., et al. (2020a). Retrospective analysis of the possibility of predicting the COVID-19 outbreak from Internet searches and social media data, China, 2020. *Eurosurveillance, 25*(10), Article 2000199.
Li, J., Chu, B., Chai, N., et al. (2021). Work resumption rate and migrant workers' income during the COVID-19 Pandemic. *Frontiers in Public Health, 9*, 464.
Li, Z., Li, X., Porter, D., et al. (2020b). Monitoring the spatial spread of COVID-19 and effectiveness of control measures through human movement data: Proposal for a predictive model using big data analytics. *JMIR Research Protocols, 9*(12), e24432.
Lian, X., Huang, J., Huang, R., et al. (2020). Impact of city lockdown on the air quality of COVID-19-hit of Wuhan city. *Science of the Total Environment, 742*, Article 140556.
Liang, S., Leng, H., Yuan, Q., et al. (2021). Impact of the COVID-19 pandemic: Insights from vacation rentals in twelve mega cities. *Sustainable Cities and Society, 74*, Article 103121.
Liao, W., Liu, X., Wang, D., et al. (2017). The impact of energy consumption on the surface urban heat island in China's 32 major cities[J]. *Remote Sensing, 9*(3), 250.
Liu, C., Liu, Z., & Guan, C. (2021). The impacts of the built environment on the incidence rate of COVID-19: A case study of King County, Washington. *Sustainable cities and society, 74*, Article 103144.
Liu, J., Zhou, J., Yao, J., et al. (2020a). Impact of meteorological factors on the COVID-19 transmission: A multi-city study in China. *Science of the total environment, 726*, Article 138513.
Liu, Q., Sha, D., Liu, W., et al. (2020b). Spatiotemporal patterns of COVID-19 impact on human activities and environment in mainland China using nighttime light and air quality data. *Remote Sensing, 12*(10), 1576.
Liu, Z., Ciais, P., Deng, Z., et al. (2020c). Near-real-time monitoring of global CO_2 emissions reveals the effects of the COVID-19 pandemic. *Nature Communications, 11*(1), 1–12.
Ma, Y., Zhao, Y., Liu, J., et al. (2020). Effects of temperature variation and humidity on the death of COVID-19 in Wuhan, China. *Science of the total environment, 724*, Article 138226.
Maiti, A., Zhang, Q., Sannigrahi, S., et al. (2021). Exploring spatiotemporal effects of the driving factors on COVID-19 incidences in the contiguous United States. *Sustainable Cities and Society, 68*, Article 102784.
Maliszewska M., Mattoo A., Van Der Mensbrugghe D. The potential impact of COVID-19 on GDP and trade: A preliminary assessment. World Bank Policy Research Working Paper, 2020 (9211).
Mirzaei, P. A., & Haghighat, F. (2010). Approaches to study urban heat island–abilities and limitations. *Building and environment, 45*(10), 2192–2201.
Nanda, D., Mishra, D. R., & Swain, D. (2021). COVID-19 lockdowns induced land surface temperature variability in mega urban agglomerations in India. *Environmental Science: Processes & Impacts, 23*(1), 144–159.
Notteboom, T., Pallis, T., & Rodrigue, J. P. (2021). Disruptions and resilience in global container shipping and ports: The COVID-19 pandemic versus the 2008–2009 financial crisis. *Maritime Economics & Logistics, 23*(2), 179–210.
Pal, S., Das, P., Mandal, I., et al. (2021). Effects of lockdown due to COVID-19 outbreak on air quality and anthropogenic heat in an industrial belt of India. *Journal of Cleaner Production, 297*, Article 126674.
Parida, B. R., Bar, S., Kaskaoutis, D., et al. (2021). Impact of COVID-19 induced lockdown on land surface temperature, aerosol, and urban heat in Europe and North America. *Sustainable Cities and Society*, Article 103336.
Parolin, Z., & Wimer, C. (2020). Forecasting estimates of poverty during the COVID-19 crisis. *Poverty and Social Policy Brief, 4*(8).
Peng, Z., Wang, R., Liu, L., et al. (2020). Exploring urban spatial features of COVID-19 transmission in Wuhan based on social media data. *ISPRS International Journal of Geo-Information, 9*(6), 402.
Phelan, P. E., Kaloush, K., Miner, M., et al. (2015). Urban heat island: mechanisms, implications, and possible remedies. *Annual Review of Environment and Resources, 40*, 285–307.
Portela, C. I., Massi, K. G., Rodrigues, T., et al. (2020). Impact of urban and industrial features on land surface temperature: Evidences from satellite thermal indices. *Sustainable Cities and Society, 56*, Article 102100.
Pulella, A., & Sica, F. (2021). Situational awareness of large infrastructures using remote sensing: The Rome–Fiumicino Airport DURING the COVID-19 lockdown. *Remote Sensing,, 13*(2), 299.
Rumpler, R., Venkataraman, S., & Göransson, P. (2020). An observation of the impact of CoViD-19 recommendation measures monitored through urban noise levels in central Stockholm, Sweden. *Sustainable Cities and Society, 63*, Article 102469.
Sailor, D. J. (2011). A review of methods for estimating anthropogenic heat and moisture emissions in the urban environment. *International Journal of Climatology, 31*(2), 189–199.
Sathe, Y., Gupta, P., Bawase, M., et al. (2021). Surface and satellite observations of air pollution in India during COVID-19 lockdown: Implication to air quality. *Sustainable Cities and Society, 66*, Article 102688.
Si, H., Shen, L., Liu, W., et al. (2021). Uncovering people's mask-saving intentions and behaviors in the post-COVID-19 period: Evidence from China. *Sustainable Cities and Society, 65*, Article 102626.
Sha, D., Malarvizhi, A. S., Liu, Q., et al. (2020). A state-level socioeconomic data collection of the United States for COVID-19 research. *Data, 5*(4), 118.
Shao, Z., Tang, Y., Huang, X., et al. (2021). Monitoring work resumption of Wuhan in the COVID-19 epidemic using daily nighttime light. *Photogrammetric Engineering & Remote Sensing, 87*(3), 195–204.
Shariati, M., Mesgari, T., Kasraee, M., et al. (2020). Spatiotemporal analysis and hotspots detection of COVID-19 using geographic information system. *Journal of Environmental Health Science and Engineering, 18*(2), 1499–1507.
Shi, P., Dong, Y., Yan, H., et al. (2020). Impact of temperature on the dynamics of the COVID-19 outbreak in China. *Science of the total environment, 728*, Article 138890.
Shakibaei, S., De Jong G, C., Alpkökin, P., et al. (2021). Impact of the COVID-19 pandemic on travel behavior in Istanbul: A panel data analysis. *Sustainable Cities and Society, 65*, Article 102619.
Sun, R., Wang, Y., & Chen, L. (2018). A distributed model for quantifying temporal-spatial patterns of anthropogenic heat based on energy consumption. *Journal of Cleaner Production, 170*, 601–609.
Tang, E., Peng, C., & Xu, Y. (2018). Changes of energy consumption with economic development when an economy becomes more productive. *Journal of Cleaner Production, 196*, 788–795.
Tian, S., Hu, N., Lou, J., et al. (2020). Characteristics of COVID-19 infection in Beijing. *Journal of infection, 80*(4), 401–406.
Tian, X., An, C., Chen, Z., et al. (2021). Assessing the impact of COVID-19 pandemic on urban transportation and air quality in Canada. *Science of the Total Environment, 765*, Article 144270.
Verbesselt, J., Hyndman, R., Newnham, G., et al. (2010). Detecting trend and seasonal changes in satellite image time series. *Remote sensing of Environment, 114*(1), 106–115.
Vidya, C. T., & Prabheesh, KP. (2020). Implications of COVID-19 pandemic on the global trade networks. *Emerging Markets Finance and Trade, 56*(10), 2408–2421.
Vîrghileanu, M., Săvulescu, I., Mihai, B. A., et al. (2020). Nitrogen dioxide (NO_2) pollution monitoring with Sentinel-5P satellite imagery over Europe during the coronavirus pandemic outbreak. *Remote Sensing, 12*(21), 3575.
Wang, P., Chen, K., Zhu, S., et al. (2020). Severe air pollution events not avoided by reduced anthropogenic activities during COVID-19 outbreak[J]. *Resources, Conservation and Recycling, 158*, Article 104814.
Wang, Q., & Li, S. (2021). Nonlinear impact of COVID-19 on pollutions–Evidence from Wuhan, New York, Milan, Madrid, Bandra, London, Tokyo and Mexico City. *Sustainable Cities and Society, 65*, Article 102629.
Wang, Q., & Zhang, F. (2021). What does the China's economic recovery after COVID-19 pandemic mean for the economic growth and energy consumption of other countries? *Journal of Cleaner Production, 295*, Article 126265.
Watts, L. M., & Laffan, S. W. (2014). Effectiveness of the BFAST algorithm for detecting vegetation response patterns in a semi-arid region. *Remote Sensing of Environment, 154*, 234–245.
Willberg, E., Järv, O., Väisänen, T., et al. (2021). Escaping from cities during the covid-19 crisis: Using mobile phone data to trace mobility in Finland. *ISPRS International Journal of Geo-Information, 10*(2), 103.
WHO. Coronavirus Disease (COVID-19) Pandemic. Available online: https://www.who.int/emergencies/diseases/novel-coronavirus-2019 (last access date: 1 July 2021).
World Bank. Global economic prospects, June 2020[J]. 2020.
WTO. Trade set to plunge as COVID-19 pandemic upends global economy. Available online: https://www.wto.org/english/news_e/pres20_e/pr855_e.htm (last access date: 1 July 2021).
Xiong, C., Hu, S., Yang, M., et al. (2020). Mobile device data reveal the dynamics in a positive relationship between human mobility and COVID-19 infections. *Proceedings of the National Academy of Sciences, 117*(44), 27087–27089.
Xu, X., Wang, S., Dong, J., et al. (2020). An analysis of the domestic resumption of social production and life under the COVID-19 epidemic. *PloS one, 15*(7), Article e0236387.

Yi, M., Loeb, N., Lin, P., et al. (2020). Assessing the influence of COVID-19 on Earth's radiative balance. *Earth and Space Science Open Archive ESSOAr*.
Zhou, C., Su, F., Pei, T., et al. (2020). COVID-19: challenges to GIS with big data. *Geography and Sustainability, 1*(1), 77–87.
Zhu, B., Zheng, X., Liu, H., et al. (2020). Analysis of spatiotemporal characteristics of big data on social media sentiment with COVID-19 epidemic topics. *Chaos, Solitons & Fractals, 140*, Article 110123.